Cellulose (2021) 28:11247–11259
https://doi.org/10.1007/s10570-021-04214-w

ORIGINAL RESEARCH

RISM-assisted analysis of role of alkali metal hydroxides in the solvation of cellulose in alkali/urea aqueous solutions

Eugene Huh · Ji-Hyun Yang · Chang-Ha Lee · Ik-Sung Ahn · Byung Jin Mhin

Received: 19 April 2021 / Accepted: 16 September 2021 / Published online: 27 October 2021

Abstract The three-dimensional reference interaction site model theory with the Kovalenko–Hirata closure (3D-RISM–KH) combined with the Kirkwood–Buff integral (KBI) was used to clarify the role of alkali metal hydroxides (MOHs) in cellulose solvation in alkali/urea aqueous solutions. Pair distribution functions, KBI, and the excess number of MOHs showed that M^+ hydrates were formed close to cellulose and that their distance was the same as the distance between M^+ ions and water molecules in the hydrates. The most stable Li^+ hydrate due to the highest Li^+ charge density was the closest to the cellulose resulting in the most electrostatic interaction and possibly hydrogen bonding with the cellulose. However, K^+ had the lowest charge density, formed the least stable hydrate, and had the least interaction with the cellulose. Hence, the direct solvation energy, which is part of the cellulose solvation energy and accounts for the solute–solvent interaction, was the most negative in the LiOH/urea solution. The solvent reorganization energy—which is another part of the cellulose solvation energy and arises from the clustering of urea, water, and MOH (i.e., ion hydrates) around cellulose—was the most negative in the LiOH/urea solution because of the highest probability and the closest positioning of the Li^+ hydrate to the cellulose. Therefore, the calculation results obtained using 3D-RISM–KH and KBI explained the difference among the cellulose solubilities in the LiOH/urea, NaOH/urea, and KOH/urea aqueous solutions.

Keywords Cellulose · Reference interaction site model (RISM) · Kirkwood–Buff integral (KBI) · Alkali metal hydroxide · Urea

Supplementary Information The online version contains supplementary material available at (https://doi.org/10.1007/s10570-021-04214-w).

E. Huh · J.-H. Yang · C.-H. Lee · I.-S. Ahn (✉)
Department of Chemical and Biomolecular Engineering, Yonsei University, Seoul 120-749, South Korea
e-mail: iahn@yonsei.ac.kr

E. Huh
e-mail: eugeneh55@gmail.com

J.-H. Yang
e-mail: prji17@naver.com

C.-H. Lee
e-mail: leech@yonsei.ac.kr

B. J. Mhin (✉)
Department of Chemistry, Pai Chai University, Daejeon 302-735, South Korea
e-mail: mhin@pcu.ac.kr

Introduction

Alkali solutions are widely used to dissolve cellulose. Alkali hydroxides in the form of hydrates have been suggested to break the intra- and intermolecular hydrogen bonds in cellulose chains and form new hydrogen bonds, thereby solvating cellulose (Cai et al.

2008; Medronho and Lindman 2014, 2015). Recently, aqueous solutions of urea (or thiourea) and various alkali metal hydroxides (e.g., LiOH, NaOH, and KOH) have shown different solvation capabilities toward cellulose molecules of varying molecular weights (Cai et al. 2004, 2005, 2008; Jiang et al. 2014; Jin et al. 2007; Wang et al. 2017a, b, c). Cellulose molecules exhibiting viscosity-average molecular weights of 4.5, 11.5, and 37.2 $\times$ 10^4 were soluble in a 4.2 % (w/w) LiOH/12 % (w/w) urea solution precooled to −10 °C (Cai and Zhang 2005). Although a 7 % (w/w) NaOH/12 % (w/w) urea solution dissolved the first two cellulose molecules, a 9.8 % (w/w) KOH/12 % (w/w) urea solution did not dissolve any of the tested cellulose molecules. Using differential scanning calorimetry, Wang et al. (2017b) estimated the feasibility of cellulose solvation at approximately −5 °C in LiOH/urea solutions and − 20 °C in NaOH/urea solutions. By measuring pulsed field-gradient spin-echo nuclear magnetic resonance (NMR) peak intensities, Wang et al. calculated that the ratios of Li^+ and Na^+ bound to cellulose were 14.3 and 4.8 %, respectively. These experimental results indicate that the interactions of these ions with cellulose and their contribution to cellulose solvation both decrease in the order $Li^+ > Na^+ > K^+$.

Furthermore, molecular dynamics (MD) simulation results suggested that the interaction between cellulose and alkali metal hydroxides such as LiOH and NaOH is primarily electrostatic. According to the calculations of Wang et al., Li^+ ions were closer than Na^+ ions to the cellulose, and the average distance between Li^+ and the cellulose oxygen atoms was shorter than between Na^+ and the same. The probability of finding Li^+ ions within the same distance of the cellulose was higher than that of finding Na^+ ions (Wang et al. 2017b; Xiong et al. 2013) investigated the dissolution of cellobiose, a unit of cellulose, in alkali solutions to clarify the role of alkali metal hydroxides in cellulose solvation. In the ^{13} C-NMR spectra of the cellobiose, a more prominent downfield chemical shift and shorter ^{13} C relaxation time were detected in the descending order LiOH > NaOH > KOH. This means that alkali metal hydroxides share the same interaction mode with cellulose and that the magnitude of the interaction is of the same order, which is consistent with the contribution of alkali metal ions to cellulose solvation. In addition, Xiong et al. stated that cellulose dissolution seemed to be considerably affected by the stability of the cation-hydration shell. The stable hydration shells of Li^+ and Na^+ allow them to form a stable complex with cellulose. However, K^+ has a weak hydration shell and cannot form a stable complex with cellulose. Therefore, the KOH solution swells rather than dissolving cellulose (Xiong et al. 2013).

In our previous work (Huh et al. 2020), the three-dimensional reference interaction site model theory with the Kovalenko–Hirata closure (3D-RISM–KH) was applied to calculate the solvation energy of cellulose in a NaOH/urea aqueous solution at 261, 280, and 298 K and to determine the contribution of each solvent species (i.e., Na^+, OH^-, urea, and water) to cellulose solvation. NaOH and urea were found along the hydrophilic edge and above and below the hydrophobic cellulose pyranose rings, respectively. Water molecules were closer to both the hydrophilic and hydrophobic moieties of the cellulose in the presence of urea than in the absence of urea, suggesting that NaOH and especially urea might attract water molecules around the cellulose to form a cluster consisting of NaOH, urea, and water, thereby stabilizing the cellulose. As a result, adding urea reduced both the solvent reorganization energy of the cellulose from 163 to −1198 kcal/mol and the interaction energy between the cellulose and the solvent by more than 100 kcal/mol. Both energies increased with increasing temperature, which accounted for the exothermic solvation of the cellulose.

In this work, a cellulose solvation system was extended to aqueous solutions of urea and various alkali metal hydroxides such as LiOH, NaOH, and KOH. The objective of this work was to determine the role of alkali metal hydroxides in cellulose solvation (i.e., their affinity to cellulose) by calculating and comparing the distribution of the solvent species, partial molar volume of the solute, and solvation energy of the cellulose. For this purpose, 3D-RISM–KH (Gusarov et al. 2012; Kovalenko 2013, 2017; Kovalenko and Gusarov 2018) was combined with the Kirkwood–Buff integral (KBI) (Giambaşu et al. 2014, 2015; Krüger et al. 2013) in this study.

Methods

The KBI (G_γ) is defined as the spatial integral over the pair distribution function ($g_\gamma^{uv}(r)$) as follows:

$$G_\gamma = \int_V [g_\gamma^{uv}(r) - 1]dr \quad (1)$$

where superscripts u and v denote the solute and solvent, respectively, V is the system volume over which the integration is carried out, and r is the distance between the solute and the solvent species. $g_\gamma^{uv}(r)$ is the ratio of the probability of finding solvent species γ at r, which is determined from the 3D-RISM calculations, to the probability of finding γ in the bulk solvent. The G_γ unit is the volume per solute molecule (Å^3/molecule). G_γ indicates the accessibility of γ to the solute, which is correlated with the affinity of γ for the solute (Nicol et al. 2017; Wernersson et al. 2015). The KBI is considered appropriate for describing all types of intermolecular interactions necessary for determining the thermodynamic properties of a solution. For example, it has been used to calculate the excess number of γ around a single solute molecule (N_γ^{excess}) as follows (Shimizu 2004, 2013):

$$N_\gamma^{excess} = \rho_\gamma(G_\gamma + V_C) \quad (2)$$

where ρ_γ is the number density of γ, and V_C is the excluded volume of the solute. The sum of G_γ and V_C corresponds to the real volume in which γ can exist near the solute. The excess number of various solvent species allows us to compare their interactions with the solute.

The partial molar volume of the solute ($\bar{V}$) provides important information about the structure of the dissolved solute and its interaction with the solvent species (Chalikian and Breslauer 1996; Imai 2007a, b; Patel et al. 2011). For an infinitely diluted solute–solvent system, $\bar{V}$ is defined as follows:

$$\bar{V} = V_C + V_I + V_{id}, \quad (3)$$

$$V_C = V_M + V_T = V_W + V_V + V_T, \quad (4)$$

where V_I and V_{id} denote the interaction volume and the ideal fluctuation volume, respectively. V_{id} is caused by the translational degrees of freedom of the solvent (Imai 2007a). V_C, which is also called the cavity volume, consists of the region occupied by the solute (V_M, the geometric volume) and an empty border region between the solute and the unaltered, uniform pure solvent (V_T, the thermal volume) (Lee 1983; Patel et al. 2011). V_M is the sum of the van der Waals volume (V_W) and void volume (V_V). V_C and its components are shown schematically in Fig. 1. Thermally induced molecular vibrations of the solute and solvent species cause the solvent to further expand. V_T, believed to be generated by this expansion, is an empty thermal volume around the solute (Chalikian and Breslauer 1996; Imai 2007a). This is correlated with the nonpolar interaction between the solute and the solvent species (i.e., more nonpolar interactions reduce V_T). V_I represents the change in the solvent volume due to intermolecular electrostatic interactions and hydrogen bonding between the cellulose and the solvent species (Chalikian and Breslauer 1996). More polar interactions between the solute and the solvent species reduce V_I. Once $\bar{V}$, V_C, V_M (the sum of V_W and V_V), and V_{id} were calculated (see the Supplementary Information for the detailed calculation methods), V_I and V_T were determined using Eqs. (3) and (4), respectively. The contributions of each solvent species to V_C and V_I were calculated separately. Because V_M is constant regardless of the solvent, the contribution of a solvent species to V_C implies its contribution to V_T. For example, $V_{C,urea}$ is the portion of V_C caused by urea and implies the relative contribution of urea to V_T. $V_{I,MOH}$ indicates the portion of V_I caused by the polar interaction of MOH with the solute cellulose.

The solvation energy (ΔE) and solvation entropy ($T\Delta S$), which are needed to calculate the excess chemical potential ($\Delta\mu$), are defined as the sum of the solute–solvent interaction (uv) and solvent–solvent reorganization (R) terms as follows:

$$\Delta E = E^{uv} + \Delta E^R \quad (5)$$

$$T\Delta S = T\Delta S^{uv} + T\Delta S^R = T\Delta S^{uv} + \Delta E^R \quad (6)$$

Because ΔE^R and $T\Delta S^R$ result from the change in the solvent–solvent interaction upon the insertion of the solute molecule (Ben-Naim 1978; Gallicchio et al. 2000; Lazaridis 2000; Misin 2017), they have the same values. Then

$$\Delta\mu = \Delta E - T\Delta S = E^{uv} - T\Delta S^{uv} \quad (7)$$

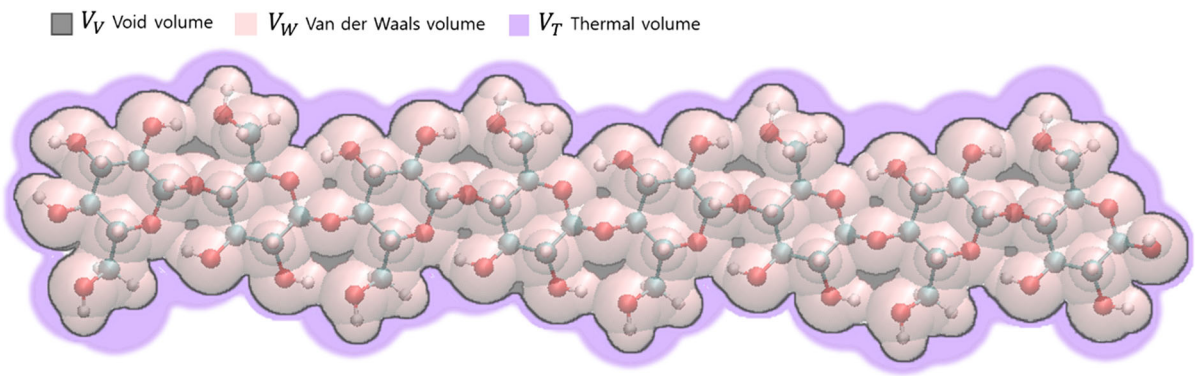

Fig. 1 Cavity volume (V_C) of cellulose composed of van der Waals volume (V_W; pink), void volume (V_V; gray), and thermal volume (V_T; purple)

3D-RISM highly overestimates the excess chemical potential (Misin 2017; Sergiievskyi et al. 2014) showed that this is primarily caused by a high solvent pressure, which leads to the overestimation of the solute insertion work. Misin (2017) argued that the water molecules near a large solute molecule, such as cellulose, undergo substantial reorganization. The density of the water molecules immediately next to the solute is lower than that of bulk water molecules, which is caused by the lack of attractive interactions with the hydrophobic moiety of the solute. Instead, they are strongly drawn in close to bulk water, forming a strong tetrahedral network. These solvent reorganizations create large cavities near the hydrophobic moieties of the solute. Such a dewetting transition cannot be considered using conventional 3D-RISM and requires pressure-corrected 3D-RISM (Misin 2017). $\Delta\mu_{PC+}$, or $\Delta\mu$ corrected by including the advanced pressure correction (PC+) and the partial molar volume of cellulose, is expressed as follows:

$$\Delta\mu_{PC+} = \Delta\mu + (P_{id} - P)\bar{V} \tag{8}$$

where P_{id} is the ideal gas pressure of the solvent given by $P_{id} = \rho_{Tot} k_B T$, and P is given by $P = \frac{1}{2} k_B T \left(\frac{1}{k_B T \chi_T} + N_{site} \rho_{Tot} \right)$. ρ_{Tot} and N_{site} are the number densities of all the solvent species and the number of sites (i.e., atoms) in the solvent, respectively (Misin et al. 2016; Sergiievskyi et al. 2014).

3D-RISM–KH calculations and MD simulations were performed using the AMBER16 package (Case et al. 2010). An Iβ-structured cellulose molecule exhibiting a polymerization degree of 8 was selected as the model in this study as in the previous one (Huh et al. 2020). Although the breakage of the hydrogen bonds and the partial deprotonation of the cellulose in strongly alkaline solutions reportedly cause structural changes (Bialik et al. 2016; Cai et al. 2008; Medronho and Lindman 2014, 2015), the Iβ-structural constraint was imposed in this study to separately investigate the effects of the different solvent species on cellulose solvation rather than to determine the combined effects of the solvent species and the cellulose structure. The following solvents were tested for cellulose solvation at 261 K: LiOH/urea aqueous solution (LU), NaOH/urea (NU), KOH/urea (KU), pure water (WO), urea aqueous solution (UO), LiOH solution (LO), NaOH solution (NO), and KOH solution (KO). The latter five solvents were used for comparison with the first three (LU, NU, and KU).

For a meaningful comparison of the cellulose solvation thermodynamics and solvent affinities toward the cellulose, the water, MOH, and urea number ratio was maintained at 27.75:1:1. The 3D-RISM–KH calculations were performed based on a 32 × 40 × 72 Å^3 box with a 0.5 Å spacing. Transferable intermolecular potential 3P (TIP3P) water was used to model the solvent water. The detailed calculation method is described in the accompanying Supplementary Information. The initial density and pressure for each solvent are listed in Table S1 (see the Supplementary Information). The force-field parameters and partial charges were assigned using the general amber force field (GAFF) and the Austin model with bond and charge correction (AM1-BCC) charge model, respectively (Jakalian et al. 2000, 2002). The structure of the model cellulose molecule was generated using a cellulose builder

(Gomes and Skaf 2012). The geometric volume (V_M) of the cellulose was calculated using Protein Volume 1.3 (Chen and Makhatadze 2015).

The 3D-RISM calculation method used in this study assumes that the model cellulose is dissolved in all the tested solvents. However, this assumption does not match the experimental finding that real cellulose is insoluble in the KOH/urea aqueous solution. However, 3D-RISM combined with KBI is expected to provide calculation results concerning the distribution of the solvent species around cellulose, its interactions with cellulose, and its contribution to the cellulose solvation energy. Such calculation results would allow the roles of the alkali metal hydroxides in cellulose solvation to be determined, which is the objective of this work.

Results and discussion

Affinities of Li^+, Na^+, and K^+ toward cellulose

Figure 2 shows an example of the pair distribution functions used in Eq. (1). In the RISM calculation, LiOH, NaOH, and KOH were all assumed to be completely dissociated into M^+ and hydroxide ions. To compare the proximity of M^+ ions to cellulose (i.e., to compare their interaction with cellulose), the pair distribution function between M^+ and O2 (or O3) atoms on the hydrophilic edge of the cellulose ($g_\gamma^{uv}(r)$) was calculated, as shown in Fig. 2a. For comparison, the pair distribution function between the M^+ and water O atoms ($g_\gamma^{vv}(r)$) was calculated and is shown in Fig. 2b. The positions of the first peaks in Fig. 2a and b (i.e., the distances between the closest M^+ ion and the cellulose O2 (or O3) atom and between the closest M^+ ion and the water O atom in M^+ hydrates, respectively) are identical for the same metal ion and increased in the order Li^+ ($\sim$ 2.0 Å) < Na^+ ($\sim$ 2.5 Å) < K^+ ($\sim$ 2.8 Å). The smaller ions (see Table S2 in the Supplementary Information) have a higher charge density and form more stable hydrates through stronger interactions with water molecules at shorter distances. The positions of the first peaks in Fig. 2a indicate that an M^+ ion approaches the cellulose as an ion hydrate and that the electrostatic interaction between the M^+ ion and the cellulose is the same as that between the M^+ ion and the water molecules in the ion hydrate, which are also capable of forming hydrogen bonds with the cellulose. The heights of the first peaks in Fig. 2a and b)indicate that the probability of finding an M^+ ion near the cellulose decreases in the order $Li^+ > Na^+ > K^+$, which is the same order as the M^+-hydrate stability. Hence, the cellulose interacts with the M^+ hydrates in the MOH/urea aqueous solutions. Because of their relatively small ionic radii, Li^+ and Na^+ can form ion hydrates more tightly than K^+. The more stable Li^+ and Na^+ hydrates formed at a higher number density closer to the cellulose contribute to the cellulose solvation, while the relatively unstable K^+ hydrates formed at the lower number density do not, which is consistent with the study findings of Xiong et al. (2013).

The KBI (G_γ) values were calculated for all the solvent species in the different solvents and are shown in Fig. 3. The negative G_γ values arise because of the excluded volume (V_C) of the cellulose (Sergiievskyi et al. 2014), and solvent species exhibiting a more negative $G_\gamma$have a lower probability of existing near and are less accessible to the cellulose. G_γ decreased in the order urea > > LiOH > water > NaOH > KOH. G_{urea} seems to be constant regardless of the other solvent species, such as MOHs, which corresponds well with the positioning of the urea above and below the pyranose rings of the cellulose and the interaction between the urea and the cellulose independent of the MOH (Huh et al. 2020; Wernersson et al. 2015; Xiong et al. 2013). G_{MOH} decreased in the order LiOH > NaOH > KOH regardless of whether urea was present in the solvent, which corresponds to the heights of the first peaks in Fig. 2a and S1 in the Supplementary Information. G_{LiOH} was higher than G_{water} in solvents LO and LU, while G_{NaOH} and G_{KOH} were lower than G_{water}. Li^+, Na^+, and K^+ have the same charge but different ionic radii increasing in the order $Li^+ < Na^+ < K^+$ (see Table S2 in the Supplementary Information). Hence, Li^+ is most easily accessible to cellulose, which enables the strongest electrostatic interaction and hydrogen bonding with cellulose and corresponds well with the experimental finding that cellulose is most favorably soluble in the LU solvent. Because of these differences in the electrostatic interaction and hydrogen bonding among the MOHs and cellulose, G_{water} was the lowest for the LiOH- containing solvent and the highest for the KOH- containing one regardless of the presence of urea (see Fig. 2).

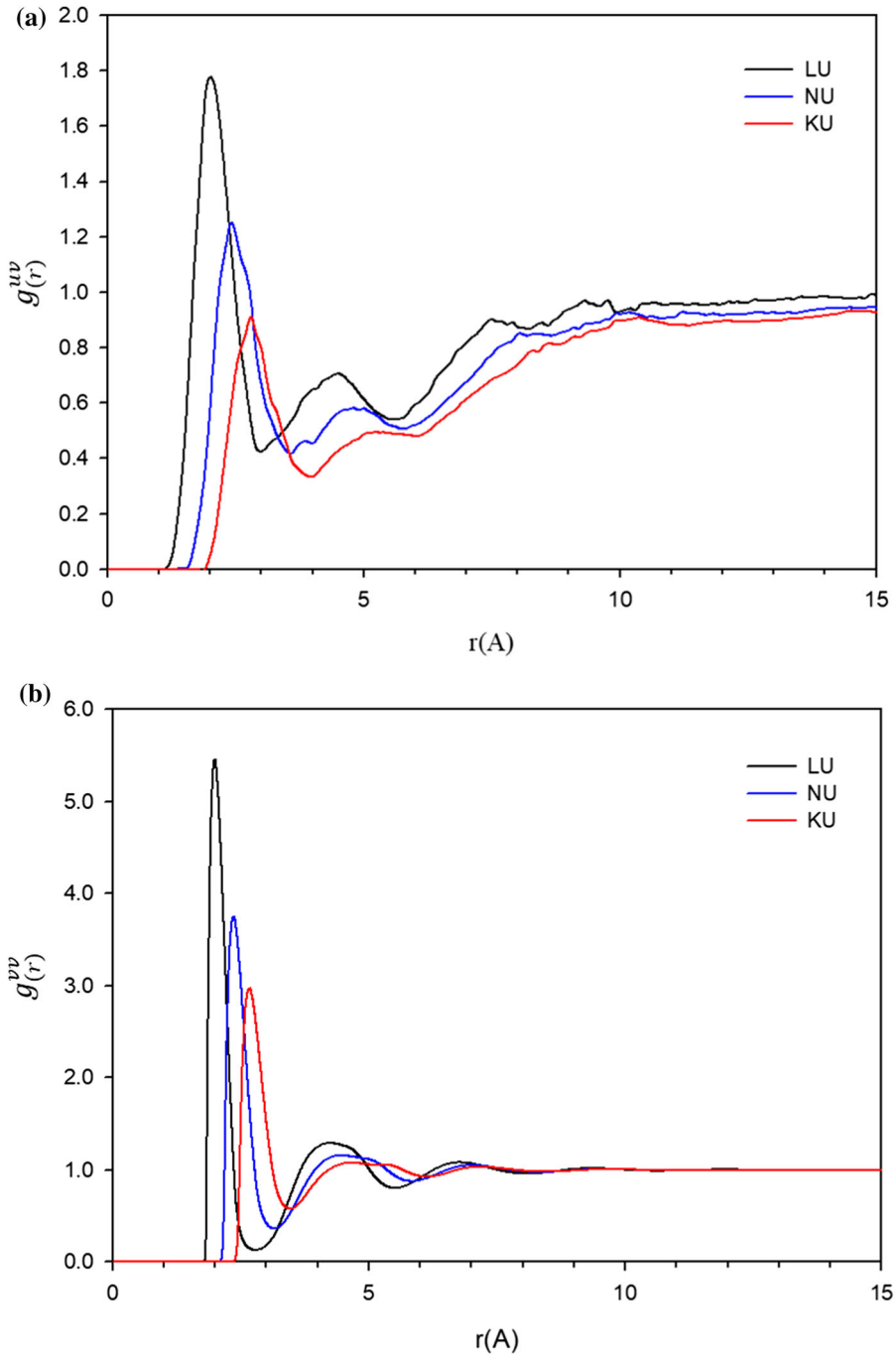

Fig. 2 (**a**) Pair distribution functions ($g^{vv}_{\gamma}(r)$) of Li^+, Na^+, and K^+ for cellulose O2 (O3) atoms in LU, NU, and KU. (**b**) Pair distribution functions ($g^{uv}_{\gamma}(r)$) of Li^+, Na^+, and K^+ for water O atoms in LU, NU, and KU. Refer to Fig. 2 of Huh et al. (2020) for cellulose O2 atoms

Table 1 summarizes the N^{excess}_{γ} of each solvent species in the different solvents. The N^{excess}_{γ} values for the cellulose in solvents WO, LO, NO, and KO are listed in Table S4. As expected from G_{MOH}, the smaller alkali metal ion yielded a higher N^{excess}_{MOH} (i.e., $N^{excess}_{LiOH} > N^{excess}_{NaOH} > N^{excess}_{KOH}$). A higher ion concentration close to the cellulose implies stronger interaction between the corresponding metal ion and the cellulose.

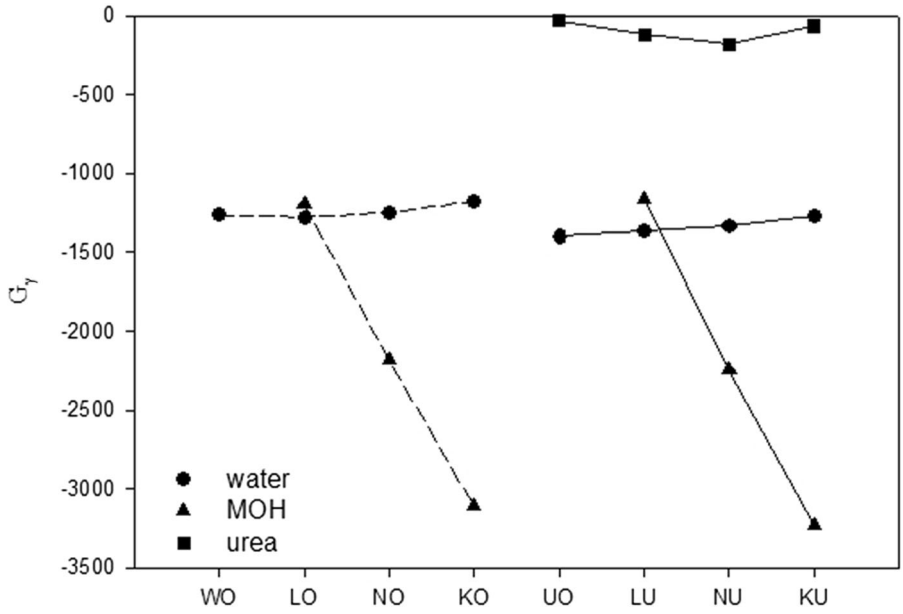

Fig. 3 Kirkwood–Buff Integral (G_γ) for solvent species γ in water (●), alkali metal hydroxide (MOH) (▲), and urea (■). G_γ unit is Å^3 per cellulose molecule

Table 1 Excess numbers of solvent species γ (N_γ^{excess}) in various solvents

Solvent	Water	LiOH/NaOH/KOH	Urea
LU	– 0.8	0.0	1.4
NU	0.4	– 1.2	1.3
KU	2.4	– 2.3	1.5
UO	– 1.2		1.5

Because urea is positioned above and below the cellulose pyranose rings, the region near the cellulose accessible to water decreases upon adding urea to the solvent. Hence, N_{water}^{excess} was lower in the urea-containing solvent. Because the size of the ion hydrates (see Table S2 in the Supplementary Information) and the interaction between the cellulose and the ion hydrates decreased in the order $Li^+ > Na^+ > K^+$, N_{water}^{excess} depended on the MOH type as follows: N_{water}^{excess} for the LiOH-containing solvent $< N_{water}^{excess}$ for the NaOH-containing solvent $< N_{water}^{excess}$ for the KOH-containing solvent (see Table 1; Fig. 4). Because urea and MOH do not compete for the same locations near the cellulose, the probability of finding MOHs around the entire cellulose molecule is not much affected by urea. Hence, the value of N_{MOH}^{excess} is similar regardless of whether the solvent contains urea, as shown by the data listed in Table 1 and S4. Based on G_γ and N_γ^{excess}, the positioning of the solvent species around a single cellulose molecule is schematically depicted in Fig. 4. MOHs and urea can hydrophilically and hydrophobically interact with cellulose, respectively (Huh et al. 2020).

Alkali-metal-hydroxide-dependent partial molar volume of cellulose

V_M, V_W, and V_V were calculated as 1173.3, 1061.7, and 111.6 Å^3, respectively. Because V_M is constant regardless of the solvent, the difference in V_C for different solvents originates from the difference in V_T. Because V_T is calculated as the difference between V_C and V_M (i.e., $V_T = V_C - V_M$), the contribution of each solvent species to V_T cannot be determined separately. Instead, V_C can be divided into the following components: $V_{C,water}$, $V_{C,MOH}$, and $V_{C,urea}$.

V_C and its components were calculated for each solvent species γ ($V_{C,\gamma}$) in LU, NU, and KU and are listed in Tables 2 and 3, respectively. Because urea and MOH were positioned close to the hydrophobic and hydrophilic parts of the cellulose, respectively (Huh et al. 2020), the $V_{C,urea}$ values were not affected

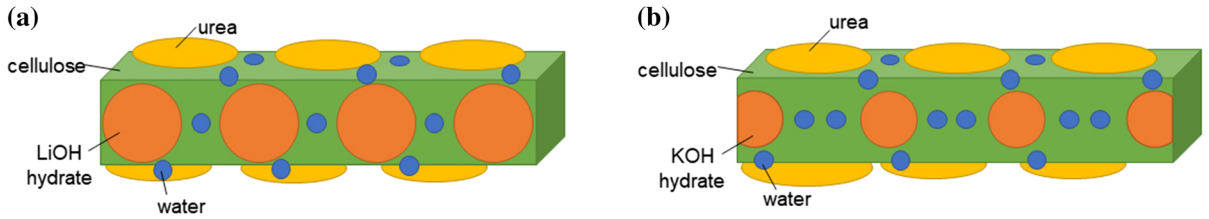

Fig. 4 Schematic depiction of solvent species around single cellulose molecule in LU (**a**) and KU (**b**). Urea (*yellow circles*) and hydrated MOH (*orange circles*) are near hydrophobic and hydrophilic parts of cellulose, respectively. Note differences in numbers of MOHs and water molecules (*blue circles*) between (**a**) and (**b**)

by the MOHs (see Table 3). The radial distribution functions of the Li^+, Na^+, and K^+ ions, shown in Fig. 2a, indicate a denser and more proximal distribution of Li^+ ions than Na^+ and K^+ ones near the cellulose. Hence, G_{MOH} and N_{MOH}^{excess} decreased in the order LiOH > NaOH > KOH. The MOHs smaller and closer to the cellulose are apt to induce thermal fluctuation more easily between the cellulose and solvent molecules, thereby further reducing V_C and increasing $V_{C,MOH}$ in the order $V_{C,LiOH} < V_{C,NaOH} < V_{C,KOH}$. Because the magnitudes of G_{water} and N_{water}^{excess} both increased in the order LU < NU < KU, $V_{C,water}$ decreased in the order LU > NU > KU. The V_C values in LO, NO, and KO are listed in Table S5, while $V_{C,water}$ and $V_{C,MOH}$ in the same solvents are listed in Table S6. Significant differences were not found in $V_{C,MOH}$ whether urea was present in the solvents or not. For the same MOH, $V_{C,water}$ was smaller in the presence of urea. This is consistent with the results of a previous study, which indicated that water molecules were positioned closer to the cellulose in the presence of urea (Huh et al. 2020). This also implies that urea facilitates thermally induced molecular fluctuations between cellulose and water.

The interaction volume (V_I) and its component for each solvent species γ ($V_{I,\gamma}$) were calculated for the cellulose in LU, NU, and KU and are listed in Tables 2 and 3, respectively. V_I increased in the order LU (i.e., the most negative) < NU < KU (i.e., the least negative), implying that the most closely distributed LiOH (see Fig. 2a) results in the most hydrophilic interaction with the cellulose. When $V_{I,water}$, $V_{I,MOH}$, and $V_{I,urea}$ were separately calculated, the difference in V_I could not be explained by $V_{I,MOH}$ among the different solvents. Although G_{MOH} and N_{MOH}^{excess} both decreased in the order LiOH > NaOH > KOH, LU exhibited the least negative $V_{I,MOH}$ and the most negative $V_{I,water}$ despite G_{water} and N_{water}^{excess} both decreasing in the order KOH > NaOH > LiOH, suggesting that MOHs may not be directly involved in hydrophilic interactions with cellulose. Instead, a portion of the water molecules were close to the cellulose; for example, the water molecules comprising ion hydrates might predominantly participate in electrostatic interactions and hydrogen bonding with the cellulose, which explains the results obtained for $V_{I,water}$ and $V_{I,MOH}$, as listed in Table 3. Because the ideal fluctuation volume (V_{id}) was negligible compared to V_C and V_I (see Table 2), its influence on $\bar{V}$ could be ignored. The V_I values in LO, NO, and KO are listed in Table S5, while $V_{I,water}$ and $V_{I,MOH}$ in the same solvents are listed in Table S6. In contrast to the urea-containing solvents, although the differences among the $V_{I,MOH}$ were negligible, the differences among the $V_{I,water}$ were significant (see Table 3 and S6), suggesting that urea facilitates the polar interactions between the cellulose and water.

Table 2 Cavity volume (V_C), interaction volume (V_I), ideal fluctuation volume (V_{id}), and partial molar volume ($\bar{V}$) of cellulose in LU, NU, and KU. [a]

Solvent	V_C	V_I	V_{id}	$\bar{V}$	V_T [b]
LU	1335.0	–57.5	1.5	1278.8	161.7
NU	1339.4	–57.4	1.4	1283.4	166.1
KU	1347.1	–50.5	1.3	1297.7	173.8
UO[c]	1360.5	–48.7	1.8	1313.6	187.2

[a] $\bar{V} = V_C + V_I + V_{id}$. Unit is $Å^3$ per cellulose molecule

[b] V_T is thermal volume calculated from $V_T = V_C - V_M$, where $V_M = 1173.3Å^3$

[c] Data for UO are given for comparison

Table 3 $V_{C,\gamma}$ and $V_{I,\gamma}$, components of V_C and V_I, for solvent species γ[a]

Solvent	$V_{C,water}$	$V_{C,MOH}$	$V_{C,urea}$	$V_{I,water}$	$V_{I,MOH}$	$V_{I,urea}$
LU	1234.7	16.4	84.0	− 50.9	− 3.5	− 3.4
NU	1210.1	45.0	84.3	− 49.9	− 4.0	− 3.4
KU	1186.6	75.1	85.4	− 43.4	− 4.2	− 3.0
UO[b]	1277.7		82.8	− 45.9		− 2.8

[a]Unit is Å^3 per cellulose molecule. V_C and V_I values are listed in Table 2

[b]Data for UO are given for comparison

Alkali-metal-hydroxide-dependent cellulose solvation thermodynamics

The solvation energies and entropies of the cellulose in LU, NU, and KU are listed in Table 4, while those of the cellulose in LO, NO, and KO are listed in Table S7. Superscripts *uv* and *R* denote that the corresponding energy terms consider solute–solvent interaction and solvent reorganization (i.e., solvent–solvent interaction), respectively. The solvation energy accounted for the experimental results obtained for the cellulose solvation (i.e., the cellulose dissolved the easiest in LU and was insoluble in KU). The E^{uv} (direct solvation energy) for LU was −481.4 kcal/mol and was lower than −470.9 and − 50.7 kcal/mol for NU and KU, respectively, which is correlated with the finding that Li^+ is positioned the closest to the cellulose and, therefore, experiences the strongest interaction with it. The $T\Delta S^{uv}$ for LU is − 518.7 kcal/mol and higher (i.e., less negative) than those for the other solvents, which indicates that the LiOH access is less hindered than the NaOH and KOH ones to the cellulose.

Note that the difference in E^{uv} was predominantly affected by the MOHs than by the water (as indicated by comparing the numbers in the brackets and parentheses in the column for E^{uv} in Table 4). The following ΔE^{uv}_{MOH-WO} and ΔE^{uv}_{MOH-UO} were calculated to determine the effect of the urea on the MOH contributions to E^{uv} (see Table 5):

$$\Delta E^{uv}_{MOH-WO} = E^{uv}(solventLO, NO, KO) - E^{uv}(solventWO) \quad (9)$$

$$\Delta E^{uv}_{MOH-UO} = E^{uv}(solventLU, NU, KU) - E^{uv}(solventUO) \quad (10)$$

Table 4 Solvation energies and entropies of cellulose in LU, NU, and KU at 261 K[a]

Solvent	ΔE	E^{uv}	$\Delta E^R(\approx T\Delta S^R)$	$T\Delta S$	$T\Delta S^{uv}$
LU	− 1672.4	− 481.4	− 1191.0	− 1709.8	− 518.7
		(− 411.8)	(− 1086.0)		(− 460.6)
		[− 49.7]	[− 101.2]		[− 29.3]
NU	− 1600.9	− 470.9	− 1130.0	− 1658.8	− 528.8
		(− 415.0)	(− 1067.3)		(− 471.2)
		[− 36.1]	[− 61.7]		[− 27.9]
KU	− 1537.9	− 450.7	− 1087.2	− 1631.5	− 544.3
		(− 403.9)	(− 1054.7)		(− 482.7)
		[− 26.9]	[− 33.2]		[− 30.2]
UO[b]	− 142.2	− 306.6	164.3	− 231.9	− 67.6
		(− 287.4)	(159.7)		(− 51.0)

[a]$\Delta E = E^{uv} + \Delta E^R$ and $T\Delta S = T\Delta S^{uv} + T\Delta S^R$. Superscripts *uv* and *R* denote solute–solvent interaction and solvent reorganization (i.e., solvent–solvent interaction), respectively. Numbers in parentheses and brackets indicate contributions of water and MOHs, respectively. Unit of energy is kcal/mol of cellulose

[b]Data for UO are given for comparison

As listed in Table 5, ΔE^{uv}_{MOH-UO} is much more negative than ΔE^{uv}_{MOH-WO}, and the difference is largest when the MOH is LiOH. The water molecules attracted toward the cellulose by the urea (Huh et al. 2020) must have participated in the formation of the M^+ hydrates near the cellulose. Because Li^+ forms the most stable hydrates, LU should show the largest increase in the interaction with the cellulose (i.e., the most negative $\Delta E^{uv}_{LiOH-UO}$ listed in Table 5). Hence, urea is believed to strengthen the interaction between the cellulose and the MOHs (i.e., M^+ hydrates), especially LiOH, which is consistent with the results shown in Fig. 2a and b.

Table 4 lists the contributions of the water and MOHs to the ΔE^R (see the numbers in parentheses and brackets in the column for ΔE^R). The reorganization of the water and MOHs around the cellulose is favored by the MOH type in the descending order LiOH > NaOH > KOH. The following $\Delta\Delta E^R_{MOH-WO}$ and $\Delta\Delta E^R_{MOH-UO}$ were calculated to determine the effect of the urea on the contribution of the MOHs to the ΔE^R (see Table 5):

$$\Delta\Delta E^R_{MOH-WO} = \Delta E^R(solventLO, NO, KO) - \Delta E^R(solventWO) \quad (11)$$

$$\Delta\Delta E^R_{MOH-UO} = \Delta E^R(solventLU, NU, KU) - \Delta E^R(solventUO) \quad (12)$$

ΔE^R was much lower for the urea-containing solvent than for the urea-free one (see Table 4 and S6). Notably, ΔE^R decreased by approximately 1300 kcal/mol in the presence of urea. As a result, $\Delta\Delta E^R_{MOH-UO}$ was much more negative than $\Delta\Delta E^R_{MOH-WO}$, and the difference was the largest when the MOH was LiOH, suggesting that urea induces the reorganization of the water and the MOHs, especially the LiOH, around the cellulose to favor solvent–solvent interactions.

The chemical potentials of the cellulose solvation were corrected by including advanced pressure correction (PC+) and are listed in Table 6 (see the $\Delta\mu_{PC+}$ column). The $\Delta\mu_{PC+}$ values are − 193.8, −188.6, and −178.4 kcal/mol for LU, NU, and KU, respectively. The $\Delta\mu_{PC+}$ for the urea-free solvent is listed in Table S8 and is higher (i.e., less negative) than that for the corresponding urea-containing solvent (e.g., − 39.8 and −193.8 kcal/mol for LO and LU, respectively). Note that the difference in $\Delta\mu_{PC+}$ among the MOHs is negligible for the urea-free solvents. Even $\Delta\mu_{PC+}$ was calculated as approximately the same for both LO and WO. Reportedly, structural changes are necessary to dissolve cellulose in strongly alkaline urea-free solutions (Bialik et al. 2016; Cai and Zhang 2005, 2008; Medronho and Lindman 2014, 2015). The Iβ-structural constraint imposed in this study seemed to generate the results listed in Table S8, which is difficult to accept. However, $\Delta\mu_{PC+}$ (as listed in Table 6) agrees with the experimental cellulose solvation results, implying that cellulose solvation in MOH/urea aqueous solutions can be explained without considering the structural changes in the cellulose. The E^{uv}, ΔE^R, and $\Delta\mu_{PC+}$ calculation results indicate that cellulose solvation in alkali/urea aqueous solutions is feasible because of the presence of urea in the solvent and that the contribution of the MOHs decreased in the order LiOH > NaOH > KOH. Although the effects of the cellulose structure (such as cellulose crystallinity and the dissociation of the cellulose chains) were not considered in this study, they will be considered as possible cellulose solvation factors in future studies.

Table 5 Effects of MOHs and urea on direct solvation energy (*uv*) and solvent reorganization energy (*R*)[a]

MOH	ΔE^{uv}_{MOH-WO}	ΔE^{uv}_{MOH-UO}	$\Delta\Delta E^R_{MOH-WO}$	$\Delta\Delta E^R_{MOH-UO}$
LiOH	–7.2	–174.8	–3.8	–1355.3
NaOH	–4.9	–164.3	16.5	–1294.3
KOH	–3.7	–144.1	28.2	–1251.5

[a]These energies were calculated at 261 K, and their unit is kcal/mol of cellulose. ΔE^{uv}_{MOH-WO}, ΔE^{uv}_{MOH-UO}, $\Delta\Delta E^R_{MOH-WO}$, and $\Delta\Delta E^R_{MOH-UO}$ are defined in Eqs. (9–12)

Table 6 Chemical potentials of cellulose solvation without ($\Delta\mu$) and with ($\Delta\mu_{PC+}$) advanced pressure correction (PC+) in LU, NU, and KU at 261 K[a]

MOH	$\Delta\mu$	$\Delta\mu_{PC+}$
LU	37.4	–193.8
NU	57.9	–188.6
KU	93.7	–178.4
UO[b]	89.7	–107.9

[a]Unit of energy is kcal/mol of cellulose

[b]Data for UO are given for comparison

Conclusions

Alkali metal hydroxides (MOHs) favored cellulose solvation in aqueous urea solutions in the descending order LiOH > NaOH > KOH, as determined based on the average molecular weights of the soluble cellulose and solvation temperatures. 3D-RISM combined with KBI was used in this study to determine the roles of the different MOHs in the dissolution of cellulose in aqueous urea solutions. Therefore, the access and interaction between the MOHs and the cellulose were estimated by calculating the pair distribution functions, KBIs, and excess number of MOHs around the cellulose. The calculation results indicated the formation of M^+ hydrates close to the cellulose. The distance between the cellulose and the closest M^+ ions was the same as that between the M^+ ions and the water molecules in the M^+ hydrate. The Li^+ hydrate, which was the most stable because of the high charge density of the Li^+ ions, was positioned the closest to the cellulose, thereby enabling the Li^+ ions to form the strongest electrostatic interaction and possibly hydrogen bonding with the cellulose. Because the K^+ ions formed the least stable hydrate owing to the lowest charge density, the K^+ hydrate was positioned the farthest from and had the weakest interaction with the cellulose. The cavity and interaction volumes of the cellulose, which are the dominant components of the partial molar volume of the cellulose, increased in the order LiOH/urea < NaOH/urea < KOH/urea. It is believed that more of the thermally induced molecular fluctuation and the polar interaction with the cellulose were induced by the MOH (i.e., M^+ hydrate) closer to the cellulose. The direct solvation energy, which is part of the cellulose solvation energy and accounts for the solute–solvent interaction, was the most negative for the LiOH/urea because of the strongest interaction between the cellulose and the LiOH. The Li^+ hydrate showed the highest probability of existing near and was positioned the closest to the cellulose, suggesting that the solvent reorganization energy—another part of the cellulose solvation energy—arises from the clustering of urea, water, and MOH (i.e., ion hydrates) around the cellulose and was the most negative for LiOH/urea. The stability, probability, and proximity of the ion hydrates to the cellulose all decreased in the order $Li^+ > Na^+ > K^+$, resulting in the solvation energy showing the opposite trend (i.e., the LiOH/urea aqueous solution exhibited the most negative solvation energy). 3D-RISM–KH combined with KBI generated important quantitative information regarding the distribution and interaction of the MOHs with the cellulose, clarified the roles of the MOHs (especially LiOH) in cellulose solvation, and helped explain the preferential dissolution of the cellulose in the LiOH/urea aqueous solutions.

Acknowledgments This work was supported by Yonsei University and Pai Chai University, and we would like to thank Elsevier for English language editing.

Declarations

Conflict of interest The authors declare that they have no known competing financial interests or personal relationships that could have influenced the work reported in this paper.

Ethical approval This study did not involve any experiments on human subjects or animals.

References

Ben-Naim A (1978) Standard thermodynamics of transfer. Uses misuses. J Phys Chem 82:792–803

Bialik E, Stenqvist B, Fang Y, Östlund Å, Furo I, Lindman BR, Lund M, Bernin D (2016) Ionization of cellobiose in aqueous alkali and the mechanism of cellulose dissolution. J Phys Chem Lett 7:5044–5048

Cai J, Zhang L (2005) Rapid dissolution of cellulose in LiOH/urea and NaOH/urea aqueous. Solut Macromol Biosci 5:539–548

Cai J, Zhang L, Zhou J, Li H, Chen H, Jin H (2004) Novel fibers prepared from cellulose in NaOH/urea aqueous solution. Macromol Rapid Comm 25:1558–1562

Cai J, Zhang L, Liu S, Liu Y, Xu X, Chen X, Chu B, Guo X, Xu J, Cheng H, Han C, Kuga S (2008) Dynamic self-assembly

induced rapid dissolution of cellulose at low temperatures. Macromolecules 41:9345–9351
Case D, Betz R, Cerutti D, Cheatham T, Darden T, Duke R AMBER16, 2016 San Francisco
Chalikian TV, Breslauer KJ (1996) On volume changes accompanying conformational transitions. Biopolymers 39:619–626
Chen CR, Makhatadze GI (2015) ProteinVolume: calculating molecular van der Waals and void volumes in proteins. BMC Bioinf 16:1–6
Edward JT, Farrell PG (1975) Relation between van der Waals and partial molar volumes of organic molecules in water. Can J Chem 53:2965–2970
Gallicchio E, Kubo M, Levy RM (2000) Enthalpy – entropy and cavity decomposition of alkane hydration free energies: Numerical results and implications for theories of hydrophobic solvation. J Phys Chem B 104:6271–6285
Giambaşu GM, Gebala MK, Panteva MT, Luchko T, Case DA, York DM (2015) Competitive interaction of monovalent cations with DNA from 3D-RISM. Nucleic Acids Res 43:8405–8415
Giambaşu GM, Luchko T, Herschlag D, York DM, Case DA (2014) Ion counting from explicit-solvent simulations and 3D-RISM. Biophys J 106:883–894
Gomes TC, Skaf MS (2012) Cellulose-Builder: a toolkit for building crystalline structures of cellulose. J Comput Chem 33:1338–1346
Gusarov S, Pujari BS, Kovalenko A (2012) Efficient treatment of solvation shells in 3D molecular theory of solvation. J Comput Chem 33:1478–1494
Huh E, Yang J-H, Lee C-H, Ahn I-S, Mhin BJ (2020) Thermodynamic analysis of cellulose complex in NaOH–urea solution using reference interaction site model. Cellulose 27:6767–6775
Imai T (2007a) Molecular theory of partial molar volume and its applications to biomolecular systems. Condens Matter Phys 10:343–361
Imai T, Ohyama S, Kovalenko A, Hirata F (2007b) Theoretical study of the partial molar volume change associated with the pressure-induced structural transition of ubiquitin. Protein Sci 16:1927–1933
Jakalian A, Bush BL, Jack DB, Bayly CI (2000) Fast, efficient generation of high-quality atomic charges. AM1-BCC model: I. Method. J Comput Chem 21:132–146
Jakalian A, Jack DB, Bayly CI (2002) Fast, efficient generation of high-quality atomic charges. AM1-BCC model: II. Parameterization and validation. J Comput Chem 23:1623–1641
Jiang Z, Fang Y, Xiang J, Ma Y, Lu A, Kang H, Huang Y, Guo H, Liu R, Zhang L (2014) Intermolecular interactions and 3D structure in cellulose–NaOH–urea aqueous system. J Phys Chem B 118:10250–10257
Jin H, Zha C, Gu L (2007) Direct dissolution of cellulose in NaOH/thiourea/urea aqueous solution. Carbohyd Res 342:851–858
Kovalenko A (2013) Multiscale modeling of solvation in chemical and biological nanosystems and in nanoporous materials. Pure Appl Chem 85:159–199
Kovalenko A (2017) Multiscale modeling of solvation. In: Breitkopf C, Swider-Lyons K (eds) Springer handbook of electrochemical energy. Springer: Heidelberg, pp 95–139
Kovalenko A, Gusarov S (2018) Multiscale methods framework: self-consistent coupling of molecular theory of solvation with quantum chemistry, molecular simulations, and dissipative particle dynamics. Phys Chem Phys 20:2947–2969
Krüger P, Schnell SK, Bedeaux D, Kjelstrup S, Vlugt TJ, Simon J-M (2013) Kirkwood–Buff integrals for finite volumes. J Phys Chem Lett 4:235–238
Lazaridis T (2000) Solvent reorganization energy and entropy in hydrophobic hydration. J Phys Chem B 104:4964–4979
Lee B (1983) Partial molar volume from the hard-sphere mixture model. J Phys Chem 87:112–118
Medronho B, Lindman B (2014) Competing forces during cellulose dissolution: from solvents to mechanisms. Curr Opin Colloid Interface Sci 19:32–40
Medronho B, Lindman B (2015) Brief overview on cellulose dissolution/regeneration interactions and mechanisms Adv Coll Interface Sci 222:502–508
Misin M (2017) Can approximate integral equation theories accurately predict solvation thermodynamics? Ph.D. thesis, University of Strathclyde
Misin M, Vainikka PA, Fedorov MV, Palmer DS (2016) Salting-out effects by pressure-corrected 3D-RISM. J Chem Phys 145:194501
Nicol TW, Isobe N, Clark JH, Shimizu S (2017) Statistical thermodynamics unveils the dissolution mechanism of cellobiose. Phys Chem Chem Phys 19:23106–23112
Patel N, Dubins DN, Pomes R, Chalikian TV (2011) Parsing partial molar volumes of small molecules: a molecular dynamics study. J Chem Phys B 115:4856–4862
Sergiievskyi VP, Jeanmairet G, Levesque M, Borgis D (2014) Fast computation of solvation free energies with molecular density functional theory: Thermodynamic-ensemble partial molar volume corrections. J Phys Chem Lett 5:1935–1942
Shimizu S (2004) Estimating hydration changes upon biomolecular reactions from osmotic stress, high pressure, and preferential hydration experiments. Proc Natl Acad Sci USA 101:1195–1199
Shimizu S, Booth JJ, Abbott S (2013) Hydrotropy: binding models vs. statistical thermodynamics. Phys Chem Chem Phys 15:20625–20632
Wang S, Sun P, Zhang R, Lu A, Liu M, Zhang L (2017a) Cation/macromolecule interaction in alkaline cellulose solution characterized with pulsed field-gradient spin-echo NMR spectroscopy. Phys Chem Chem Phys 19:7486–7490
Wang S, Lyu K, Sun P, Lu A, Liu M, Zhuang L, Zhang L (2017b) Influence of cation on the cellulose dissolution investigated by MD simulation and experiments. Cellulose 24:4641–4651
Wang S, Sun P, Liu M, Lu A, Zhang L (2017c) Weak interactions and their impact on cellulose dissolution in an alkali/urea aqueous system. Phys Chem Chem Phys 19:17909–17917

Wernersson E, Stenqvist B, Lund M (2015) The mechanism of cellulose solubilization by urea studied by molecular simulation. Cellulose 22:991–1001

Xiong B, Zhao P, Cai P, Zhang L, Hu K, Cheng G (2013) NMR spectroscopic studies on the mechanism of cellulose dissolution in alkali solutions. Cellulose 20:613–621